NUSC Reprint Report 6350
1 February 1985

Performance of Constrained Estimation for Tracking with a Linear Array

John G. Baylog
Antonio A. Magliaro
Kai F. Gong
Sherry E. Hammel

Combat Control Systems Department

Naval Underwater Systems Center
Newport, Rhode Island / New London, Connecticut

Reprint of an article published in the IEEE 1984 Conference Record of the Eighteenth Asilomar Conference on Circuits, Systems and Computers, Pacific Grove, California.

PERFORMANCE OF CONSTRAINED ESTIMATION FOR TRACKING WITH A LINEAR ARRAY

John G. Baylog
Antonio A. Magliaro
Kai F. Gong
Sherry E. Hammel

U.S. Naval Underwater Systems Center
Newport, R.I. 02841

ABSTRACT

This paper addresses passive contact tracking using measurements from a perturbed multiple element linear array. Time delay measurements of ray path range differences between array sensors are considered where sensor positions are perturbed off the mean array axis. Estimator performance is analyzed and it is shown that under large range-to-baseline conditions, uncertain array position can yield unacceptable solutions. Specifically, velocity estimates are shown to be particularly sensitive to the rate of change in array shape. A method utilizing a speed constraint is proposed for compensation or reduction of estimation bias. To achieve this, general inequality constraints are incorporated into an iterative least squares estimator, and performance is demonstrated.

I. INTRODUCTION

Tracking using measurements from a linear array represents a nonlinear state estimation problem that utilizes both array and processing gains to obtain contact state estimates. Typically, this problem involves the determination of position and motion of an acoustic contact from noise corrupted time-delay measurements derived from spatially distributed sensors. Time-delay measurements are generated by cross-correlating signals received at each of the subarrays as shown in figure 1 for a three element array. The array of sensors can be stationary or attached to a mobile observer. In either case, large separations between sensors provide the baseline necessary for good tracking performance. However, the problem is complicated when the precise location of each sensor is uncertain.[1] When the array is being trailed behind a mobile observer, lateral array motion can result from perturbations in observer velocity as well as from environmentally induced excitations distributed along the array. Hence, inaccurate array shape assumptions can induce modelling errors into the estimation process.

The contact state estimation problem addressed here is not amenable to simple solution since intrinsic system nonlinearities preclude the application of conventional linear estimation techniques. Estimation algorithms based on a first order linearization approximation that employ an anomaly-free array model have been developed.[2,3] In the presence of array motion mismodelling, imprecise array shape parameterization can induce significant errors in contact state estimates. Under these conditions, estimation accuracy can be improved via utilization of any a priori information about the contact's state. For example, previous studies have shown that for the bearings-only tracking problem, significant performance gains can be realized by constraining the contact state in the estimation process.[4,5]

This paper extends previous investigations on constrained passive localization and motion analysis to include measurements derived from a linear array in the presence of array motion mismodelling. For this application, contact-observer dynamics are modelled in a cartesian coordinate system. As in [2] and [3], contact position and velocity estimates are generated by an iterative least squares estimator that utilizes a Householder transformation to solve the Gauss-Newton equation. The algorithm can accommodate either the collinear array assumption or some other presumed array shape, and is augmented to comply with general inequality constraints. Array deformation is characterized by a lateral displacement from a collinear array at each sensor location as shown in figure 2. Displacements are mapped into parameters defining array shape, and estimator performance is characterized as a function of these parameters. For purposes of analysis, a sinusoidal array perturbation model is used to denote the difference between true and an assumed collinear array shape. A speed constraint is then imposed and the concomitant performance gains are illustrated through simulation experiments.

II. CONTACT/OBSERVER DYNAMICS AND MEASUREMENT MODEL

An absolute coordinate system is utilized for the target-observer geometry described in figure 3 where the origin is defined as the observer position at the time when the first measurement becomes available. The contact is assumed to be traveling with constant velocity. In many

tracking applications, observer maneuvers are either necessary or highly desirable to enhance system observability.[6] However, with time-delay measurements generated from a linear array, no observer maneuver is required for two-dimensional contact position and velocity estimation. To clarify the tracking aspects presented in this paper, no observer maneuver is utilized, and an infinite homogeneous underwater environment is assumed.

Acoustic hydrophones are presumed to be evenly spaced along the trailing linear array with fixed sensor separation L, as shown in figure 3. The $\bar{a}_i(k)$ vectors define relative position of the three hydrophone acoustic centers at time k with respect to the initial observer position. The $\bar{r}_i(k)$ vectors denote the spacial separation between the contact and each sensor and are given by

$$\bar{r}_i(k) = \bar{r}(k) - \bar{a}_i(k) = \begin{bmatrix} r_x(k) \\ r_y(k) \end{bmatrix} - \begin{bmatrix} a_{ix}(k) \\ a_{iy}(k) \end{bmatrix} \qquad (2.1)$$

with $r_x(k)$ and $r_y(k)$ denoting contact position in the absolute coordinate system. Time-delay measurements reflect the differences in travel time of sound propagation from the contact to each acoustic sensor. These are generated by cross-correlating the signals received at each sensor, and are modelled by

$$\tau_1(k) = (R_2(k) - R_1(k))/c + \eta_1(k) \qquad (2.2)$$

$$\tau_2(k) = (R_3(k) - R_2(k))/c + \eta_2(k) \qquad (2.3)$$

where $R_i(k) = \|\bar{r}_i(k)\|$ denotes the ray path range from contact to the i'th sensor, c is the speed of sound, and $\eta_1(k)$ and $\eta_2(k)$ denote uncorrelated zero mean additive noise components with common variance σ_η^2. A measurement of the ray path range difference for sensors 1 and 3 can also be generated but is not considered here.

Figure 2 describes the perturbation model of sensor displacement relative to a collinear array. In this figure, each $y_i(k)$ denotes perpendicular displacement from the mean array axis for each respective sensor. The $\bar{a}_i(k)$ vectors are related to the lateral displacements by the transformation

$$\bar{a}_i(k) = \begin{bmatrix} \cos C_o & \sin C_o \\ -\sin C_o & \cos C_o \end{bmatrix} \begin{bmatrix} (kTS_o - iL) \\ y_i(k) \end{bmatrix} \qquad (2.4)$$

where C_o and S_o denote observer heading and speed, respectively.

Parameters describing general array deformation in lieu of arbitrary lateral displacements are also described in figure 2. These are array distortion and rotation, viz.,

$$d(k) = y_2(k) - (y_1(k) + y_3(k))/2 \qquad (2.5)$$

$$\theta(k) = \tan^{-1}[(y_3(k) - y_1(k))/2L] , \qquad (2.6)$$

where the rotation angle $\theta(k)$ denotes angular deviation of the array from the mean array axis while the distortion d(k) describes bending of the array. With array shape defined by array distortion and rotation, displacement of sensor $y_1(k)$ merely denotes a translational displacement of the array from the mean array axis. Note that given array shape and displacement $y_1(k)$, lateral displacement of sensors 2 and 3 is given by

$$y_2(k) = y_1(k) + d(k) + L \tan\theta \qquad (2.7)$$

$$y_3(k) = y_1(k) + 2L\tan\theta . \qquad (2.8)$$

The respective displacements $y_i(k)$ are related to each other due to the physical dynamics of moving a non-rigid body through the medium.[7] For purposes of analysis, array displacements are assumed here to oscillate at frequency ω_o, and are given by

$$y_i(k) = h_i \sin(\omega_o kT - i pL) , \qquad (2.9)$$

where p represents a positional phase component. When $p = \omega_o/S_o$ and $h_i = h$ for all i, the array traces out a single curve in the absolute coordinate system as it is pulled through the medium. For this case, the displacement at one point along the array is merely a delayed version of array displacement at another point along the array. In general, array motion is a dynamic response to excitations delivered from the observer and/or distributed along the array. These excitations can be broadband or narrowband processes. By varying ω_o, estimator performance can be analyzed as a function of frequency. Hence, the spectral nature of the excitation need not be identified. Note that with this harmonic description of array motion, d(k) and $\tan(\theta(k))$ are also harmonic in the same frequency due to the linearity of equations (2.5) and (2.6) in these variables.

III. PERTURBATION ANALYSIS

At each sample time, an instantaneous localization solution is provided by directly mapping time delays into wavefront curvature range and bearing. For the case of an unperturbed array, it is easily shown that the mapping takes the form[8]

$$R = \frac{L^2 - c^2(\tau_1^2 + \tau_2^2)/2}{c(\tau_2 - \tau_1)} \qquad (3.1)$$

$$\beta = \sin^{-1}\left\{ -\frac{c(\tau_1 + \tau_2)}{2L} - \frac{c^2(\tau_1^2 - \tau_2^2)}{4RL} \right\} \qquad (3.2)$$

where R denotes contact range relative to the mid-array and β denotes the relative bearing as measured from broadside to the array, with time index k omitted. When array elements are perturbed off the mean array axis as shown in

figure 2, equations (3.1) and (3.2) no longer apply. Hence, utilizing perturbed time delays in the above mapping results in a biased localization solution.[3] The extent of this bias and its effect upon contact velocity estimates is now shown.

Consider as unperturbed time delays those noise-free measurements obtained from sensors aligned with the mean array axis. Then, as array elements are perturbed by the corresponding displacements y_i, it can be seen that the perturbed ray path ranges become

$$R_{ip} = R_i [1 + y_i(y_i - 2R_t\cos\beta_t)/R_i^2]^{1/2} \quad , i=1,2,3 \qquad (3.3)$$

where R_t and β_t represents the true (unperturbed) range and bearing. Expanding (3.3) by a second order Taylor series and using measurement equations (2.2) and (2.3), the perturbed time delays become

$$\tau_{jp} = \tau_j + \Delta\tau_j \qquad j=1,2. \qquad (3.4)$$

where

$$\Delta\tau_j = \frac{1}{2c}\left[\frac{y_{j-1}^2}{R_{j-1}} - \frac{y_j^2}{R_j} - 2R_t\cos\beta_t\left(\frac{y_{j-1}}{R_{j-1}} - \frac{y_j}{R_j}\right)\right. \qquad (3.5)$$
$$\left. - \frac{1}{8}\left(\frac{y_{j-1}^2}{R_{j-1}^3}(-y_{j-1} + 2R_t\cos\beta_t)^2 - \frac{y_j^2}{R_j^3}(-y_j + 2R_t\cos\beta_t)\right)\right]$$

represents the time delay perturbation. With $y_j \ll R_j$, and $L/R_t \ll 1$, then $R_{j-1}/R_j \approx 1$. Combining this with equations (2.5) and (2.6) yields

$$\Delta\tau_1 = -\frac{(d + L\tan\theta)\cos\beta_t}{c} \qquad (3.6a)$$

$$\Delta\tau_2 = \frac{(d - L\tan\theta)\cos\beta_t}{c} \qquad (3.6b)$$

These expressions are now used to replace τ_j with its perturbed value τ_{jp} in equations (3.1) and (3.2) to obtain

$$R = \frac{A - B(\cos\beta_t)d + EL\cos\beta_t\tan\theta - (\cos^2\beta_t)d^2 - L^2\cos^2\beta_t\tan^2\theta}{B + 2(\cos\beta_t)d} \qquad (3.7a)$$

and

$$\beta = \sin^{-1}\left(-\frac{E}{2L} + (\cos\beta_t)\tan\theta \right. \qquad (3.7b)$$
$$\left. - \frac{BE - 2E(\cos\beta_t)d + 2BL\cos\beta_t\tan\theta + 4L^2(\cos^2\beta_t)\,d\tan\theta}{4RL}\right)$$

where

$$A = L^2 - c^2(\tau_1^2 + \tau_2^2)/2$$
$$B = c(\tau_2 - \tau_1)$$
$$E = c(\tau_1 + \tau_2) \quad .$$

Using the far field approximations[4] $B \approx L^2\cos^2\beta_t/R_t$ and $E \approx -2L\sin\beta_t$, the bias in range is given by

$$\frac{\Delta R}{L} = -\left(\frac{\cos\beta_t + 2\rho^2}{\alpha} - \frac{2\rho^2}{\alpha\cos\beta_t}\right)\delta \qquad (3.8)$$
$$- \frac{2\rho\tan\beta_t}{\alpha}\tan\theta - \frac{\rho}{\alpha}\delta^2 - \frac{\rho}{\alpha}\tan^2\theta$$

where $\rho = \frac{R_t}{L}$, $\delta = \frac{d}{L}$, $\alpha = 1 + \frac{2\rho\delta}{\cos\beta_t}$.

Expanding (3.7b) using the first order Taylor series expansions for $\sin^{-1}(\bullet)$ and $1/\alpha$, the bias in bearing is

$$\Delta\beta = \left[\frac{-\cos^2\beta_t\sin\beta_t}{2\rho^3}\right]\delta + \left[1 + \frac{3\cos^2\beta_t - 2}{2\rho^2}\right]\tan\theta \qquad (3.9)$$

Biases in range rate and bearing rate can now be found by differentiating (3.8) and (3.9), viz.,

$$\frac{\Delta\dot{R}}{L} = c_1\dot{\rho} + c_2\dot{\beta}_t + c_3\dot{\delta} + c_4\dot{\theta} \qquad (3.10)$$

where

$$c_1 = \frac{1}{\alpha^2}\left[-\frac{4\rho}{\cos\beta_t}\delta - 2\tan\beta_t\tan\theta + \left(1 - \frac{4\rho^2}{\cos^2\beta_t}\right)\delta^2 - \tan^2\theta\right]$$

$$c_2 = \frac{1}{\alpha^2}\left[(\sin\beta_t - 2\rho^2\sin\beta_t)\delta - \frac{2\rho}{\cos^2\beta_t}\tan\theta + 4\rho\tan\beta_t\,\delta^2 - \frac{4\rho^2}{\cos\beta_t}\delta\tan\theta\right]$$

$$c_3 = \frac{1}{\alpha^2}\left[-(\cos\beta_t + \frac{2\rho^2}{\cos\beta_t}) - 2\rho\delta + \frac{4\rho^2\sin\beta_t}{\cos^2\beta_t}\tan\theta - \frac{2\rho^2}{\cos\beta_t}\delta^2 - \frac{2\rho^2}{\cos\beta_t}\tan^2\theta\right]$$

$$c_4 = \frac{\sec^2\theta}{\alpha^2}\left[-2\rho\tan\beta_t - 4\frac{\rho^2\sin\beta_t}{\cos^2\beta_t}\delta - 2\rho\tan\theta - \frac{4\rho^2}{\cos\beta_t}\delta\tan\theta\right]$$

and

$$\Delta\dot{\beta} = c_5\dot{\rho} + c_6\dot{\beta}_t + c_7\dot{\delta} + c_8\dot{\theta} \qquad (3.11)$$

where

$$c_5 = \left(\frac{3\cos^2\beta_t\sin\beta_t}{2\rho^4}\right)\delta - \left(\frac{3\cos^2\beta_t - 2}{\rho^3}\right)\tan\theta$$

$$c_6 = \left(\frac{2\cos\beta_t - 3\cos^3\beta_t}{2\rho^3}\right)\delta - \left(\frac{3\sin 2\beta_t}{2\rho^2}\right)\tan\theta$$

$$c_7 = -\frac{\cos^2\beta_t\sin\beta_t}{2\rho^3}$$

$$c_8 = \sec^2\theta\left[1 + \frac{3\cos^2\beta_t - 2}{2\rho^2}\right] \quad .$$

Some important observations regarding equations (3.8) through (3.11) can now be made. First, note that when $\rho \gg 1$, bearing error is dominated by unmodelled rotation θ, while rotation rate $\dot{\theta}$ dominates the bearing rate error. This is expected, considering the coordinate rotation necessary to realign the mean array axis with the actual array. At near broadside, range error is essentially determined by distortion. With $|\delta| \ll \frac{1}{\rho} < 1$, then $\alpha \approx 1$ and for small rotation and near broadside bearing

$$\left.\begin{aligned} \frac{\Delta R}{L} &= -2\rho^2\delta \\ \Delta\beta &= \tan\theta \\ \frac{\Delta\dot{R}}{L} &= -2\rho^2\dot{\delta} \\ \Delta\dot{\beta} &= \dot{\theta} \end{aligned}\right\} \quad (3.12)$$

Indeed, the product $\rho\delta$ characterizes the ill-conditioning effects induced by array motion mismodelling on localization estimates. When array shape is concave ($\delta<0$), contact range is biased long, approaching infinity for $\delta=-1/2\rho$, while for a convex array shape, range is biased short. Relative speed S can be obtained from the relation

$$S^2 = \dot{R}^2 + (R\dot{\beta})^2 \quad . \quad (3.13)$$

With the assumptions described above and the special case of zero relative speed considered in the paper, the speed error is given by

$$\frac{\Delta S}{L} = \left[4\rho^4\dot{\delta}^2 + (\rho(1-2\rho\delta)\dot{\theta})^2\right]^{1/2} \quad . \quad (3.14)$$

Note that in the decoupled cases of $\theta=0$ (no rotation) and $d=0$ (no distortion), ΔS decouples accordingly into distortion rate and rotation rate, respectively. This case clearly illustrates the potential sensitivity of speed estimates to array perturbations rates.

IV. ITERATED LEAST SQUARES

Unconstrained Estimation

While localization solutions may be obtained by direct mapping of time delays into range and bearing, estimates of contact velocity are obtained by processing time-delay measurements over several measurement samples. In either case, smoothing is desirable to reduce the effect of measurement noise. Because the measurement equations (2.1) and (2.2) are nonlinear, an iterated least squares approach similar to that described in [2] and [3] is selected to estimate contact position and velocity from the measured data. Specifically, an iterative algorithm based on conventional Gauss-Newton procedures is used to minimize the performance index (PI) given below.

Defining the contact state estimate as

$$\hat{\bar{x}} = [r_x(k_o), r_y(k_o), v_x, v_y]^T \quad (4.1)$$

with $r_x(k_o)$ and $r_y(k_o)$ representing contact position at some time k_o and (v_x, v_y) the (constant) contact velocity estimate, the performance index associated with the unconstrained estimator takes the form

$$PI(\hat{\bar{x}}) = \|\bar{f}(\hat{\bar{x}})\|^2 = \bar{f}^T(\hat{\bar{x}})\bar{f}(\hat{\bar{x}}) = \sum_{n=1}^{N} f_n^2(\hat{\bar{x}}) \qquad N>4 \quad (4.2)$$

where

$$f_n(\hat{\bar{x}}) = \left(\tau_j(k) - \hat{\tau}_j(k)\right)/\sigma_\eta = \tau_j(k)/\sigma_\eta - (\|\bar{r}(k) - \bar{a}_{j-1}(k)\| - \|\bar{r}(k) - \bar{a}_j(k)\|)/c\sigma_\eta \quad (4.3)$$

for j=1 or 2 depending upon whether n is odd (j=1) or even (j=2), and where current range is related to $\bar{r}(k_o)$ by

$$r_x(k) = r_x(k_o) + (k-k_o)Tv_x \quad (4.4a)$$

$$r_y(k) = r_y(k_o) + (k-k_o)Tv_y \quad . \quad (4.4b)$$

The iterative procedure for obtaining the contact state estimate is

$$\hat{\bar{x}}_{i+1} = \hat{\bar{x}}_i + z\bar{g}_i \quad (4.5)$$

where i is the iteration index, z is the step-size, and $\bar{g}_i$ denotes the search direction vector. Here, $\bar{g}_i$ will be found by minimizing a linearized version of the performance index which is based on a Gauss-Newton first order linearization procedure.[2,3] Specifically, this performance index takes the form

$$PI_L(\hat{\bar{x}}_i) = \|TJ(\hat{\bar{x}}_i)\bar{g}_i + T\bar{f}(\hat{\bar{x}}_i)\|^2 = \left\|\begin{bmatrix}U\\ \ddots\end{bmatrix}\bar{g}_i + \begin{bmatrix}\tilde{f}\\ \tilde{e}\end{bmatrix}\right\| \quad (4.6)$$

where $J(\hat{\bar{x}}_i)$ denotes the Jacobian of $\bar{f}(\hat{\bar{x}}_i)$ and is described in the appendix. To avoid matrix inversion, the orthogonal transformation T known as the Householder[10] has been utilized. This operation transforms the Jacobian into partitioned components consisting of an upper (4x4) matrix U and a ((N-4)x4) null matrix. The measurement residual vector $\bar{f}$ is transformed into the (4x1) vector $\tilde{f}$ and the ((N-4)x1) vector $\tilde{e}$. The search direction vector, $\bar{g}_i$, is the solution to the normal equations associated with PI_L, namely

$$\bar{g}_i = U^{-1}\tilde{f} \quad . \quad (4.7)$$

A back substitution algorithm[10] is employed to preclude inversion of U. With $\bar{g}_i$ determined, the step size z is determined as in [3]. The iteration procedure is initialized by utilizing the wavefront curvature range and bearing defined in the previous section. Specifically, time delays are mapped into positional components while contact velocity is initialized at zero. Iteration is continued until either a termination condition is detected (i.e., the percent change in PI_L falls below some threshold) or a maximum allowable number of iterations is reached (typically set at 50).

Estimation with Inequality Constraints

General inequality constraints will now be incorporated into the least squares estimator. Constrained contact state estimation requires minimization of the performance index of equation (4.2) subject to general inequality constraints of the form

$$\bar{q}_{MIN} \leq \bar{q}(\hat{\bar{x}}) \leq \bar{q}_{MAX} \quad (4.8)$$

where $\bar{q}(\hat{\bar{x}})$ denotes the vector of functionals that are to be bounded.

One approach in solving inequality constraint problems is to define slack variables of the form

$$\alpha_i^2 = (q_{i\,MAX} - q_i(\hat{x}))(q_i(\hat{x}) - q_{i\,MIN}) = b_i(\hat{x}) \qquad i=1,\ldots,M \quad (4.9)$$

The slack variable method converts minimization with inequality constraints to minimization with equality constraints since in order for α_i to be real, relation (4.8) has to be satisfied. Lagrange multipliers are used to adjoin these variables to the original PI via

$$PI_c = PI_u + \sum_{i=1}^{M} \lambda_i (\alpha_i^2 - b_i(\hat{x})) \qquad (4.10)$$

with PI_c and PI_u denoting the unconstrained and constrained performance indices, respectively. Note that for minimization of PI_c,

$$\frac{\partial PI_c}{\partial \alpha_i} = 2\alpha_i\lambda_i = 0 \quad . \qquad (4.11)$$

Furthermore, the α_i need not be directly computed, but rather can be eliminated to yield the Kuhn-Tucker conditions.[4]

$$\lambda_i b_i(\hat{x}) = 0 \qquad i=1,\ldots,M \qquad (4.12a)$$

$$\lambda_i \geq 0 \qquad i=1,\ldots,M \qquad (4.12b)$$

$$q_{i\,MIN} \leq q_i(\hat{x}) \leq q_{i\,MAX} \qquad i=1,\ldots,M \quad . \qquad (4.12c)$$

With no loss of generality, the unconstrained measurement residual vector is augmented as

$$\bar{f}(\hat{x}) = [f_1, \ldots, f_N, C_1, \ldots, C_M]^T \qquad (4.13)$$

where

$$C_i = \sqrt{\lambda_i}\; b_i(\hat{x}) \quad . \qquad (4.14)$$

The unconstrained Jacobian is augmented by an additional row for each constraint that is violated (see appendix).

Hence, the contact state estimate is obtained by applying the Gauss-Newton iterative procedure described in the previous section to the following modified performance index

$$PI_c = PI_u - \sum_{i=1}^{M} \lambda_i b_i^2(\hat{x}) \quad . \qquad (4.15)$$

When constraints are violated, iteration continues until constrained parameters reach the predetermined boundary. Selection of Lagrangian multipliers can be achieved through an iteration process as in [8]. Assuming there are no contradictory constraints and that the degree of modelling error is not so severe as to preclude realization of the constraint, then each λ_i increases in magnitude through iteration until the constraint is realized (i.e., $\lambda_i = \lambda_{io}$). Note that Lagrangian multipliers with values greater than λ_{io} have no additional effect upon the PI since $b_i(\hat{x})$ vanishes.

V. EXPERIMENTAL RESULTS

To illustrate the sensitivity of contact speed estimates to array motion mismodelling, several simulation experiments were conducted using the geometry described in figure 3. This scenario represents a parallel geometry where relative motion between contact and observer is zero and commences with the contact being broadside to the observer (β=135°). Nominal values of observer and contact speed are both set to 0.01 L/sec where L is sensor separation. A normalized initial range (R/L) of 80.0 was employed. For the first set of experiments, time-delay measurements are assumed to be noise free (i.e., SNR= ∞). Data was collected over a processing interval of 10 minutes containing a total of 100 equispaced measurements. The sinusoidal perturbation model given by equation (2.9) was used to individually describe array distortion and rotation.

Sensitivity of contact speed estimates to array perturbations is depicted in figures 4 and 5. Specifically, figure 4 depicts the sensitivity to array distortion (zero array rotation) while figure 5 depicts sensitivity to array rotation (zero array distortion). Note that for negative distortion values, the speed error peaks are shifted left at lower frequencies. Speed error curves for negative rotation angles have been omitted since they were observed to coincide with those in figure 5. The sensitivity curves are plotted as a function of normalized frequency f_n, where $\omega_e = 2\pi f_n/600$ is used in the respective perturbation models. Note that speed estimates can significantly be affected by a relatively small perturbation in rotation. Using the sinusoidal perturbation model dictates that distortion and rotation rates increase with frequency. However, the speed errors plotted in the figures are actually "smoothed" errors. Hence, speed estimates are shown to be particularly sensitive to array perturbations in a certain intermediate frequency interval. As indicated in the perturbation analysis, for $(d/L)\cdot(R/L)>1$, very large speed errors are generated; this was also observed experimentation.

The potential performance gains realized by incorporating a speed constraint are illustrated in figures 6 and 7. Performance improvement is depicted by the ratio of constrained to unconstrained contact state estimate errors. Figures 6a and 7a depict estimation with an equality speed constraint, ($S_{min} = S_{max} = S_{true}$), while 6b and 7b result from incorporating inequality constraints ($S_{min} = 0$, $S_{max} = 3S_{true}$). Note that in all these figures, estimation accuracy is significantly improved for only one contact parameter at any particular frequency. When equality constraints are imposed, improvement is realized over nearly the whole frequency spectrum. However, due to smoothing effects of the estimator, performance improvement realized from the inequality constraint is obtained only over the frequency interval where speed estimates are most sensitive to array motion modelling errors, and hence, the constraint is violated.

Figures 8 and 9 describe the effects of modelling error and improvement via the speed constraint for a Monte Carlo simulation, where the same geometry of figure 3 is used, and only distortion is considered. For this case, time delays are corrupted by zero mean white gaussian noise of variance $\sigma_\eta^2 = 2.5\times10^{-9}$, and a random phase component distributed between $(0,2\pi)$ is incorporated into the sinusoidal perturbation model. The Monte Carlo experiment consisted of 30 sample runs, from which error statistics were computed. Figure 8 describes the sensitivity of estimated speed to distortion for d/L = 0.001, and is consistent with figures 4 and 5. Figure 9a describes the improvement in mean range error for the cases where the same equality and inequality constraints described above are utilized. Figure 9b describes the improvement in range error variance for the two constraint conditions. Again these results are consistent with the single own experiment described above.

VI. SUMMARY AND CONCLUSIONS

The focus of this paper has been to (1) demonstrate the sensitivity of contact velocity estimates to array shape modelling error, and (2) to show performance improvement of contact state estimation with a speed constraint when such modelling errors are present. Specifically, sensitivity of estimated contact speed to unassumed array deformation has been demonstrated through a perturbation analysis of wavefront curvature range and bearing, yielding contact velocity as a function of actual relative velocity, shape error, and rate of change of the shape error. A sinusoidal error model was used to characterize speed error as a function of frequency to show where estimated speed is most sensitive. This sensitivity was demonstrated through simulation via an iterated least squares algorithm. Note that while the perturbation analysis describes predicted speed error, simulation results contain the low pass filtering effect of smoothing provided by the least squares estimator. The analysis was based on assuming a collinear array. However, it is expected that the same form of contact velocity sensitivity to array motion mismodelling will result for more general array shape assumptions.

Experimental results also illustrated the potential performance gains that can be achieved through utilizing a priori contact speed information. Specifically, estimation accuracy was enhanced, and the use of equality constraints was shown to provide performance improvement over the whole frequency spectrum. However, when more general inequality constraints are utilized, improvements in contact estimates occur only in the frequency intervals where they were most sensitive to array motion modelling errors.

APPENDIX

The Jacobian matrix required for solution of the Gauss-Newton equation is defined by

$$\mathbf{J}(\hat{\mathbf{x}}) = \frac{\partial \bar{f}}{\partial \hat{\mathbf{x}}} \qquad (A.1)$$

where $\bar{f}$ is the unconstrained measurement residual vector of equation (4.2) and $\hat{x}$ is as defined in equation 4.1. Each row of the Jacobian then takes the form

$$\frac{\partial f_n}{\partial \hat{\mathbf{x}}} = -\frac{\partial \hat{\tau}_j(k)}{\partial \hat{\mathbf{x}}} \qquad (A.2)$$

where j=1 for odd numbered rows and j=2 for even numbered rows, and τ_j is defined by equations (2.2) and (2.3). Let D=T(k-k_o) and

$$J_{1x} = \left(\rho_{(j+1)x}(k) - \rho_{jx}(k)\right)/C \qquad (A.3a)$$

$$J_{jy} = \left(\rho_{(j+1)y}(k) - \rho_{jy}(k)\right)/C \qquad (A.3b)$$

where

$$\bar{\rho}_j(k) = \frac{\bar{r}(k) - \bar{a}_j(k)}{|\bar{r}(k) - \bar{a}_j(k)|} \qquad j=1,2,3\,. \qquad (A.4)$$

Then each pair of rows of the Jacobian matrix is given by:

$$\begin{bmatrix} J_{1x} & J_{1y} & DJ_{1x} & DJ_{1y} \\ J_{2x} & J_{2y} & DJ_{2x} & DJ_{2y} \end{bmatrix}. \qquad (A.5)$$

The respective $\rho_i(k)$ vectors represent unit vectors emanating from each sensor and directed toward the contact at sample time k.

Violation of imposed inequality constraints requires augmentation of the residual vector and the Jacobian. When the speed constraint is violated, the unconstrained residual vector is augmented by

$$f_{N+1}(\hat{x}) = (S_{max}-S(\hat{x}))(S(\hat{x})-S_{min})$$
$$\text{where } S(\hat{x}) = [v_x^2 + v_y^2]^{1/2}. \qquad (A.6)$$

The elements of the additional row of the Jacobian matrix is given by

$$[o\ o\ kv_x/S\ \ kv_y/S] \qquad (A.7)$$

where

$$k = 2\left(\frac{S_{max} + S_{min}}{2} - S(\hat{x})\right) \qquad (A.8)$$

is proportional to the deviation from the midpoint between the constraint boundaries.

ACKNOWLEDGEMENT

The authors wish to acknowledge the efforts of Mrs. Cheryl Cote and Mrs. Jeanne Chaves for preparing the original manuscript, and the programming support provided by Mr. Marcus Graham. This work was supported by NUSC IR funds (Project A7911) and tasks 62633N and 735P80.

REFERENCES

[1] G.C. Carter, "Time-Delay Estimation for Passive Sonar Signal Processing," IEEE Trans. Acoustics, Speech and Signal Processing, Vol. ASSP-30, No. 3, June 1981.

[2] D.J. Murphy, "Target Tracking with a Linear Array in an Underwater Environment," Proceedings of 14th Asilomar Conference on Circuits, Systems, and Computers, November 1982.

[3] D.J. Murphy, B.W. Guimond and D.W. Moore, "Linear Array Tracking of a Maneuvering Target," 15th Asilomar Conference on Circuits, Systems, and Computers, November 1981.

[4] K.F. Gong, A.A. Magliaro and S.C. Nardone, "Parameter Estimation in a Constrained State Space," 17th Asilomar Conference on Circuits, Systems, and Computers, November 1983.

[5] K.F. Gong, A.G. Lindgren, and S.C. Nardone, "Passive Target Localization and Motion Analysis with a State Parameter Constraint," 15th Asilomar Conference on Circuits, Systems, and Computers, November 1981.

[6] S.C. Nardone and V.J. Aidala, "Observability Criteria for Bearings-Only Target Motion Analysis," IEEE Trans. on Aerosp. Electron. Syst., Vol. AES-17, March 1981.

[7] A.P. Paidoussis, "Dynamics of Flexible Slender Cylinders in Axial Flow," Journal of Fluid Mechanics, Vol. 26, 1966.

[8] J.C. Hassab, B.W. Guimond, S.C. Nardone, "Estimation of Location and Motion Parameters of a Moving Source Observed from a Linear Array," J. Acoust. Soc. Am., Vol 70, No. 4, October 1981.

[9] J.C. Hassab, "The Effect of Uncertainty in the Heading or Placement of a Subarray on Passive Ranging Accuracy," J. Acoust. Soc. Am., Vol 75, No. 2, February 1984.

[10] G.J. Bierman, Factorization Methods for Discrete Sequential Estimation, Academic Press, 1977.

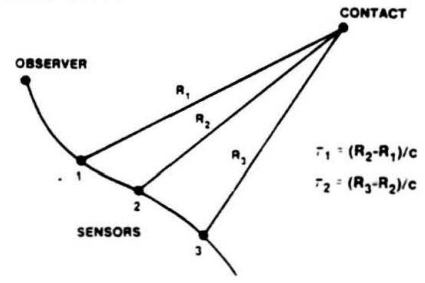

Figure 1. Tracking with a Linear Array

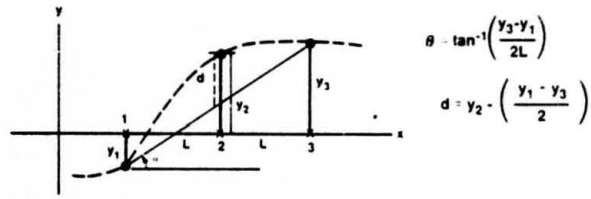

Figure 2. Array Shape Description

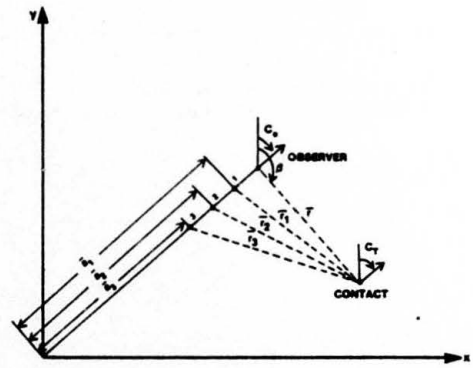

Figure 3. Scenario Description

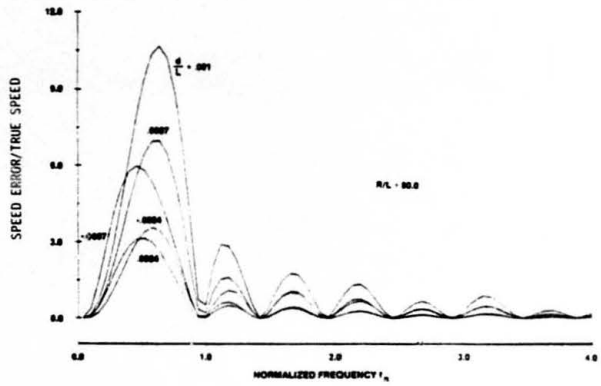

Figure 4. Sensitivity of Speed Estimate to Distortion

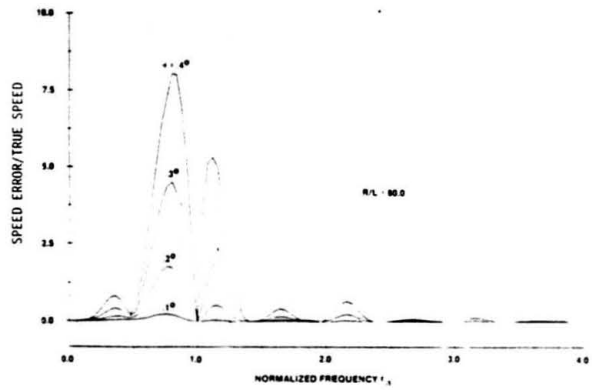

Figure 5. Sensitivity of Speed Estimate to Rotation

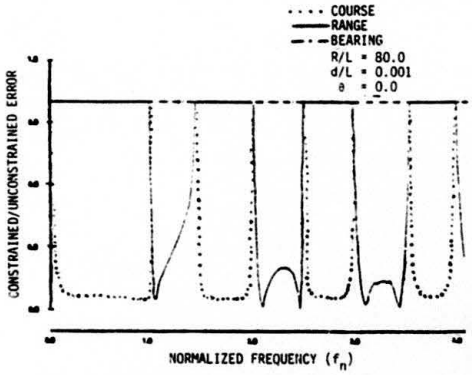

Figure 6a. Improvement via Speed Constraint in Presence of Distortion, $S_{MIN}/S_{true} = S_{MAX}/S_{true} = 1$

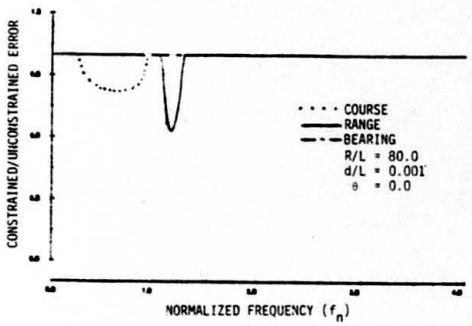

Figure 6b. Improvement via Speed Constraint in Presence of Distortion, $S_{MIN}/S_{true} = 0$, $S_{MAX}/S_{true} = 3$

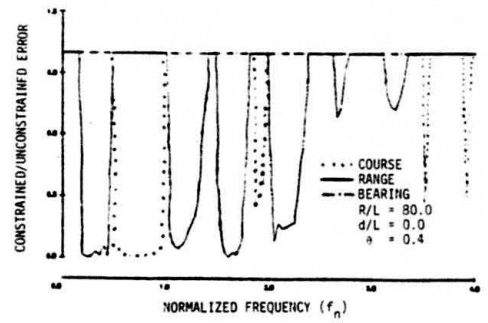

Figure 7a. Improvement via Speed Constraint in Presence of Rotation, $S_{MIN}/S_{true} = S_{MAX}/S_{true} = 1$

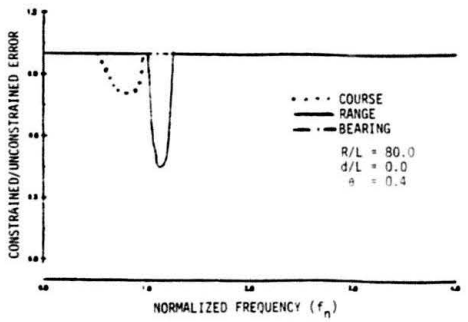

Figure 7b. Improvement via Speed Constraint in Presence of Rotation, $S_{MIN}/S_{true} = 0$, $S_{MAX}/S_{true} = 3$

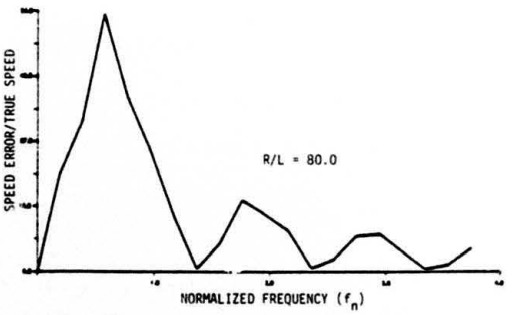

Figure 8. Sensitivity of Mean Speed Estimate to Distortion (Monte Carlo)

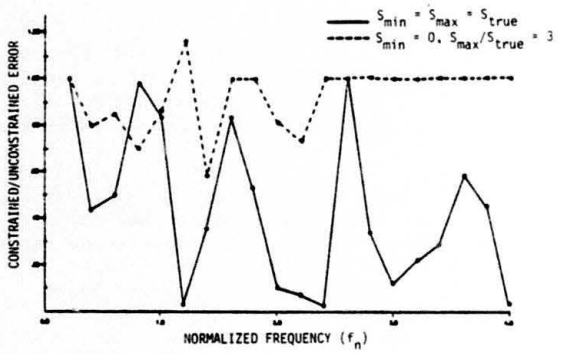

Figure 9a. Improvement in Mean Range Error via Speed Constraint in Presence of Distortion (Monte Carlo)

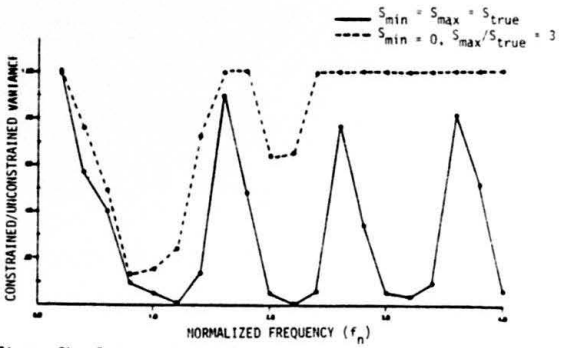

Figure 9b. Improvement in Range Error Variance via Speed Constraint in the Presence of Distortion (Monte Carlo)